

Abrikosov flux-lines in two-band superconductors with mixed dimensionality

K. Tanaka¹ and M. Eschrig²

¹*Department of Physics and Engineering Physics, University of Saskatchewan,
116 Science Place, Saskatoon, Saskatchewan, Canada S7N 5E2*

²*Institut für Theoretische Festkörperphysik and DFG-Center for Functional Nanostructures,
Universität Karlsruhe, D-76128 Karlsruhe, Germany*

We study vortex structure in a two-band superconductor, in which one band is ballistic and quasi-two-dimensional (2D), and the other is diffusive and three-dimensional (3D). A circular cell approximation of the vortex lattice within the quasiclassical theory of superconductivity is applied to a recently developed model appropriate for such a two-band system [Tanaka *et al* 2006 *Phys. Rev. B* **73** 220501(R); Tanaka *et al* 2007 *Phys. Rev. B* **75** 214512]. We assume that superconductivity in the 3D diffusive band is “weak”, i.e., mostly induced, as is the case in MgB₂. Hybridization with the “weak” 3D diffusive band has significant and intriguing influence on the electronic structure of the “strong” 2D ballistic band. In particular, the Coulomb repulsion and the diffusivity in the “weak” band enhance suppression of the order parameter and enlargement of the vortex core by magnetic field in the “strong” band, resulting in reduced critical temperature and field. Moreover, increased diffusivity in the “weak” band can result in an upward curvature of the upper critical field near the transition temperature. A particularly interesting feature found in our model is the appearance of additional bound states at the gap edge in the “strong” ballistic band, which are absent in the single-band case. Furthermore, coupling with the “weak” diffusive band leads to reduced band gaps and van Hove singularities of energy bands of the vortex lattice in the “strong” ballistic band. We find these intriguing features for parameter values appropriate for MgB₂.

I. INTRODUCTION

Vortices are complex objects even in conventional type-II superconductors, and vortex structure can reveal underlying physics of the pairing interaction. The 40 K superconductor MgB₂ [3] is the best material discovered so far for studying multiple-band superconductivity. It can be well described by a two-band model that consists of the “strong” quasi-2D σ band (energy gap ≈ 7.2 meV) and the “weak” 3D π band (energy gap ≈ 2.3 meV), and there is evidence of induced superconductivity [4, 5, 6, 7, 8] and strong impurity scattering in the π band. By tunneling along the c axis, Eskildsen *et al* have probed the vortex core structure in the π band, and have found that the local density of states (LDOS) is completely flat as a function of energy at the vortex centre, with no signature of localized states [5]. Moreover, the core size as measured by a decay length of the zero-bias LDOS was found to be much larger than expected from H_{c2} . The existence of two length scales in the vortex lattice has also been suggested by the μ SR measurement [9]. The thermal conductivity measurement [10] has detected a rapid increase of delocalized quasiparticles for field well below H_{c2} . Unusually large vortex core size and the extended nature of quasiparticle motion have also been found in the two-band superconductor NbSe₂ [11, 12, 13, 14, 15, 16]. There is the possibility of multi-band superconductivity in a number of other materials [17, 18, 19, 20, 21, 22, 23], and understanding the electronic structure in the vortex state of multiband superconductors is of great interest.

Theoretically, the vortex state in a two-band superconductor has been studied assuming both bands to be in the clean [24] and dirty [25] limit. With superconduc-

tivity (mostly) induced in one band, it has been found that there are two different length scales associated with the two bands, and that the averaged zero-bias LDOS increases rapidly as a function of field in the “weak” band. Neither of these models, however, are suitable for describing many MgB₂ samples, in which the σ and π bands are in the ballistic and diffusive limit, respectively. We have recently formulated a unique two-band model, in which one band (“ σ band”) is ballistic and the other (“ π band”) is diffusive, and there is little interband impurity scattering [1, 2]. This picture is appropriate for describing MgB₂, in which two-band superconductivity is retained even in “dirty” samples. (See extensive references in ref. [2].) Having MgB₂ in mind, in our model it is assumed that the σ and π bands are quasi-2D and 3D, respectively, and superconductivity is mostly induced in the π band through the pairing interaction with the σ band. We have examined the electronic structure around an isolated vortex and have found that the zero-bias LDOS in the π band can have a decay length much larger than in the σ band. A particularly intriguing feature that emerges in our model is the possible existence of bound states at the gap edge in the ballistic band, in addition to the well-known Caroli-de Gennes Matricon (CdM) bound states [26], in the vortex core.

In this work, we extend our two-band model to describe the vortex lattice and investigate the effects of induced superconductivity and impurities in the “weak” diffusive band on the electronic properties in the mixed state. We have found the presence of highly delocalized quasiparticles for relatively weak field, in agreement with the experiment on MgB₂ [5, 10] and the earlier theoretical works [24, 25]. Furthermore, band gaps and van Hove singularities of energy bands of the vortex lattice in the

“strong” ballistic band can be reduced by coupling with the “weak” diffusive band. There exist gap-edge bound states in the vortex core in the ballistic band – that solely arise from coupling to the diffusive band – also in the vortex lattice.

II. FORMULATION

We utilize a recently developed model appropriate for a system with coupled ballistic and diffusive bands [1, 2]. Both the ballistic and diffusive limits can be described within the quasiclassical theory of superconductivity, in which all the physical information is contained in the quasiclassical Green function, or propagator. We write the propagator in band α as $\hat{g}_\alpha(\epsilon, \vec{p}_{F\alpha}, \vec{R})$, where ϵ is the quasiparticle energy measured from the chemical potential, $\vec{p}_{F\alpha}$ the quasiparticle momentum on the Fermi surface corresponding to band α , and \vec{R} the spatial coordinate. The hat refers to the 2×2 matrix structure in the Nambu-Gor'kov particle-hole space. In the clean σ band, $\hat{g}_\sigma(\epsilon, \vec{p}_{F\sigma}, \vec{R})$ satisfies the Eilenberger equation [27, 28],

$$\left[\epsilon \hat{\tau}_3 - \hat{\Delta}_\sigma, \hat{g}_\sigma \right] + i \hbar \vec{v}_{F\sigma} \cdot \nabla \hat{g}_\sigma = \hat{0}, \quad (1)$$

where $\vec{v}_{F\sigma}$ is the Fermi velocity and $\hat{\Delta}_\sigma$ the (spatially varying) order parameter. The three Pauli matrices are denoted by $\hat{\tau}_i$, $i = 1, 2, 3$, and $[\dots, \dots]$ denotes the commutator. Motivated by the Fermi surface of MgB₂, we assume a cylindrical Fermi surface and treat the σ band as quasi-two-dimensional. The σ -band coherence length is defined as $\xi_\sigma = \hbar v_{F\sigma} / 2\pi T_c$, where T_c is the transition temperature, and used as length unit.

We assume that the π band is in the diffusive limit. In the presence of strong impurity scattering, the momentum dependence of the quasiclassical Green function is averaged out, and the equation of motion for the resulting propagator $\hat{g}_\pi(\epsilon, \vec{R})$ reduces to the Usadel equation [29],

$$\left[\epsilon \hat{\tau}_3 - \hat{\Delta}_\pi, \hat{g}_\pi \right] + \nabla \frac{\hbar \mathbb{D}}{\pi} (\hat{g}_\pi \nabla \hat{g}_\pi) = \hat{0}, \quad (2)$$

with the diffusion constant tensor \mathbb{D} . Throughout this work, we assume an isotropic tensor $\mathbb{D}_{ij} = D \delta_{ij}$ and define the π -band coherence length $\xi_\pi = \sqrt{\hbar D / 2\pi T_c}$. Both ballistic and diffusive propagators are normalized according to $\hat{g}_\sigma^2 = \hat{g}_\pi^2 = -\pi^2 \hat{1}$ [27].

The quasiparticles in different bands are assumed to be coupled only through the pairing interaction. Self-consistency for the spatially varying order parameters in the two bands is achieved through the coupled gap equations,

$$\Delta_\alpha(\vec{R}) = \sum_\beta V_{\alpha\beta} N_{F\beta} \mathcal{F}_\beta(\vec{R}), \quad (3)$$

where $\alpha, \beta \in \{\sigma, \pi\}$, and $\hat{\Delta}_\alpha = \hat{\tau}_1 \text{Re } \Delta_\alpha - \hat{\tau}_2 \text{Im } \Delta_\alpha$. The coupling matrix $V_{\alpha\beta}$ determines the pairing interaction,

$N_{F\beta}$ is the Fermi-surface density of states on band β , and

$$\begin{aligned} \mathcal{F}_\sigma(\vec{R}) &\equiv \int_{-\epsilon_c}^{\epsilon_c} \frac{d\epsilon}{2\pi i} \langle f_\sigma(\epsilon, \vec{p}_{F\sigma}, \vec{R}) \rangle_{\vec{p}_{F\sigma}} \tanh\left(\frac{\epsilon}{2T}\right), \\ \mathcal{F}_\pi(\vec{R}) &\equiv \int_{-\epsilon_c}^{\epsilon_c} \frac{d\epsilon}{2\pi i} f_\pi(\epsilon, \vec{R}) \tanh\left(\frac{\epsilon}{2T}\right). \end{aligned} \quad (4)$$

Here f_α is the upper off-diagonal (1,2) element of the matrix propagator \hat{g}_α , and ϵ_c is a cutoff energy (that will be ultimately eliminated as discussed below). The Fermi surface average over the σ -band is denoted by $\langle \dots \rangle_{\vec{p}_{F\sigma}}$. In this work, we consider isotropic s -wave coupling as is the case for MgB₂.

To study the mixed state, we introduce a circular cell approximation, meaning that we simulate the vortex unit cell by a circle. Other suggestions for circular cell approximations have been introduced in refs. [30] and [31] for the Usadel and Eilenberger equation, respectively. We assume strong type-II superconductivity, in which case the spatial variation of magnetic field within the unit cell can be neglected for fields not too close to H_{c1} . This is the case for MgB₂. We assume that magnetic field is in the $-z$ direction (taking into account that the electron charge $e < 0$, this gives a positive phase winding). The vector potential is then given by

$$\vec{A}(\vec{r}) = -\frac{H_0}{2} r \vec{e}_\phi, \quad (5)$$

with $\vec{H}_0 = -H_0 \vec{e}_z = \nabla \times \vec{A}$ and $r = \sqrt{x^2 + y^2}$. The radius of the vortex unit cell is determined by the fact that one flux quantum penetrates the unit cell,

$$H_0 \pi r_c^2 = \Phi_0, \quad (6)$$

with $\Phi_0 = hc/2|e| = \pi \hbar c / |e|$. Thus,

$$\frac{2e}{\hbar c} A_\phi(r) = \frac{r}{r_c^2}. \quad (7)$$

This can be used directly in both the Eilenberger and the Usadel equation. In both cases, the vector potential can be incorporated by the replacement

$$\nabla_i \hat{X} \rightarrow \hat{\partial}_i \hat{X} \equiv \nabla_i \hat{X} - i \left[\frac{e}{\hbar c} \hat{\tau}_3 A_i, \hat{X} \right]_\circ, \quad (8)$$

where the \circ symbol involves a time convolution if X is time-dependent; otherwise it simply implies matrix multiplication. Note that in the diffusive case this also affects the expression for the current density. This can be obtained by the requirement of local gauge invariance that the local gauge transformation

$$\hat{g} \rightarrow e^{i\chi \hat{\tau}_3} \circ \hat{g} \circ e^{-i\chi \hat{\tau}_3} \quad (9)$$

$$\vec{A} \rightarrow \vec{A} + \frac{\hbar c}{e} \nabla \chi \quad (10)$$

$$\Phi \rightarrow \Phi - \frac{\hbar}{e} \partial_t \chi \quad (11)$$

with any $\chi(\vec{r}, t)$ should leave the basic equations of motion (transport equations) invariant (in our case there is no time dependence, hence no scalar potential Φ). The vector and scalar potentials can be gauged *locally* away, by writing down the equations at any point \vec{R} with $\nabla\chi = -\frac{e}{\hbar c}\vec{A}$ and $\partial_t\chi = \frac{e}{\hbar}\Phi$. Thus, the equations with potentials can be obtained by observing that

$$\begin{aligned} & \nabla(e^{i\chi\hat{\tau}_3} \circ \hat{g} \circ e^{-i\chi\hat{\tau}_3}) = \\ & e^{i\chi\hat{\tau}_3} \circ (\nabla\hat{g} + i[\nabla\chi\hat{\tau}_3, \hat{g}]_{\circ}) \circ e^{-i\chi\hat{\tau}_3}. \end{aligned} \quad (12)$$

Now, we use the Riccati parametrization of the Green functions for both the Eilenberger [32, 33, 34, 35] and Usadel [36] equations:

$$\hat{g}_\alpha = -\frac{i\pi}{1 + \gamma_\alpha\tilde{\gamma}_\alpha} \begin{pmatrix} 1 - \gamma_\alpha\tilde{\gamma}_\alpha & 2\gamma_\alpha \\ 2\tilde{\gamma}_\alpha & \gamma_\alpha\tilde{\gamma}_\alpha - 1 \end{pmatrix}, \quad (13)$$

where $\tilde{\gamma}_\sigma(\epsilon, \vec{p}_{F\sigma}, \vec{R}) = \gamma_\sigma^*(-\epsilon^*, -\vec{p}_{F\sigma}, \vec{R})$ and $\tilde{\gamma}_\pi(\epsilon, \vec{R}) = \gamma_\pi^*(-\epsilon^*, \vec{R})$.

Because the transport equations for the Riccati amplitudes must also be invariant under any local gauge transformation, we can write them down immediately by noting that the above gauge transformation means

$$\gamma \rightarrow e^{i\chi} \circ \gamma \circ e^{-i\chi} \quad (14)$$

$$\tilde{\gamma} \rightarrow e^{-i\chi} \circ \tilde{\gamma} \circ e^{-i\chi}, \quad (15)$$

or if we have no time dependence,

$$\gamma \rightarrow e^{2i\chi}\gamma \quad (16)$$

$$\tilde{\gamma} \rightarrow e^{-2i\chi}\tilde{\gamma}. \quad (17)$$

Similarly, $\Delta \rightarrow e^{2i\chi}\Delta$ and $\Delta^* \rightarrow e^{-2i\chi}\Delta^*$. We thus obtain for the clean σ band,

$$\Delta_\sigma + 2\epsilon\gamma_\sigma + \Delta_\sigma^*\gamma_\sigma^2 + i\hbar v_{f\sigma,i}\partial_i\gamma_\sigma = 0, \quad (18)$$

with $\partial_i = (\nabla_i + 2i\nabla\chi) = (\nabla_i - i\frac{2e}{\hbar c}A_i)$, and

$$\Delta_\sigma^* - 2\epsilon\tilde{\gamma}_\sigma + \Delta_\sigma\tilde{\gamma}_\sigma^2 + i\hbar v_{f\sigma,i}\tilde{\partial}_i\tilde{\gamma}_\sigma = 0, \quad (19)$$

with $\tilde{\partial}_i = (\nabla_i - 2i\nabla\chi) = (\nabla_i + i\frac{2e}{\hbar c}A_i)$. For the dirty π band, we have [36]

$$\Delta_\pi + 2\epsilon\gamma_\pi + \Delta_\pi^*\gamma_\pi^2 - i\hbar D \left(\partial_i\partial_i\gamma_\pi - \frac{2\tilde{\gamma}_\pi(\partial_i\gamma_\pi)^2}{1 + \gamma_\pi\tilde{\gamma}_\pi} \right) = 0, \quad (20)$$

and

$$\Delta_\pi^* - 2\epsilon\tilde{\gamma}_\pi + \Delta_\pi\tilde{\gamma}_\pi^2 + i\hbar D \left(\tilde{\partial}_i\tilde{\partial}_i\tilde{\gamma}_\pi - \frac{2\gamma_\pi(\tilde{\partial}_i\tilde{\gamma}_\pi)^2}{1 + \gamma_\pi\tilde{\gamma}_\pi} \right) = 0. \quad (21)$$

We consider a vortex extending in z direction, with its centre situated at $x = y = 0$ for each z . We write $(x, y) = r(\cos\phi, \sin\phi)$ and $(v_{Fx}, v_{Fy}) = v_F(\cos\theta, \sin\theta)$, and $\Delta = |\Delta(r)|e^{i\phi}$, $\gamma = \gamma(\theta; \phi, r)e^{i\phi}$, and $\tilde{\gamma} = \tilde{\gamma}(\theta; \phi, r)e^{-i\phi}$. Then we can use the above equations with the quantities $|\Delta(r)|$, $\gamma(\theta; \phi, r)$, and $\tilde{\gamma}(\theta; \phi, r)$, and with the replacements $\partial \rightarrow (\nabla - i\frac{2e}{\hbar c}A_\phi(r)\vec{e}_\phi + i\vec{e}_\phi/r)$ and $\tilde{\partial} \rightarrow (\nabla + i\frac{2e}{\hbar c}A_\phi(r)\vec{e}_\phi - i\vec{e}_\phi/r)$. Here we have used $\nabla\phi = \vec{e}_\phi/r$.

To obtain the Riccati amplitudes in the 2D ballistic band, we must first solve for the boundary values along the unit cell circle, from which to integrate the Riccati equations along a given trajectory. To simulate the phase change across a unit cell boundary, we impose the boundary condition (here we omit the subscript σ),

$$\gamma_{in}(\theta; \phi, r_c) = -\gamma_{out}(\theta; \phi + \pi, r_c), \quad (22)$$

where *in* and *out* refer to incoming and outgoing trajectories, respectively, and similarly for $\tilde{\gamma}$. For each trajectory we solve for the boundary value γ_{in} selfconsistently.

For the 3D diffusive band, we use the symmetry

$$\gamma_\pi(\phi, r) = \gamma_\pi(0, r)e^{i\phi} \quad (23)$$

$$\tilde{\gamma}_\pi(\phi, r) = \tilde{\gamma}_\pi(0, r)e^{-i\phi}. \quad (24)$$

Then equations (20) and (21) reduce to the following dimensionless equations for $\gamma_\pi(0, r) = \gamma_\pi(r) \equiv \gamma_\pi$ and $\tilde{\gamma}_\pi(0, r) = \tilde{\gamma}_\pi(r) \equiv \tilde{\gamma}_\pi$:

$$|\Delta_\pi|(1 + \gamma_\pi^2) + 2\epsilon\gamma_\pi - i \left(\frac{\xi_\pi}{\xi_\sigma} \right)^2 \left(\partial_r^2\gamma_\pi + \frac{1}{r}\partial_r\gamma_\pi - \left(\frac{r}{r_c^2} - \frac{1}{r} \right)^2 \gamma_\pi \frac{1 - \gamma_\pi\tilde{\gamma}_\pi}{1 + \gamma_\pi\tilde{\gamma}_\pi} - \frac{2\tilde{\gamma}_\pi(\partial_r\gamma_\pi)^2}{1 + \gamma_\pi\tilde{\gamma}_\pi} \right) = 0, \quad (25)$$

$$|\Delta_\pi|(1 + \tilde{\gamma}_\pi^2) - 2\epsilon\tilde{\gamma}_\pi + i \left(\frac{\xi_\pi}{\xi_\sigma} \right)^2 \left(\partial_r^2\tilde{\gamma}_\pi + \frac{1}{r}\partial_r\tilde{\gamma}_\pi - \left(\frac{r}{r_c^2} - \frac{1}{r} \right)^2 \tilde{\gamma}_\pi \frac{1 - \gamma_\pi\tilde{\gamma}_\pi}{1 + \gamma_\pi\tilde{\gamma}_\pi} - \frac{2\gamma_\pi(\partial_r\tilde{\gamma}_\pi)^2}{1 + \gamma_\pi\tilde{\gamma}_\pi} \right) = 0, \quad (26)$$

The boundary condition in the dirty case is that the first derivative of $\gamma_\pi(r)$ and $\tilde{\gamma}_\pi(r)$ is zero at the cell boundary.

We solve for the order parameters by diagonalizing

the (cutoff dependent) interactions and thus transform-

ing the gap equations (3) into the form

$$\begin{pmatrix} \Delta^{(0)} \\ \Delta^{(1)} \end{pmatrix} = \begin{pmatrix} \lambda^{(0)} & 0 \\ 0 & \lambda^{(1)} \end{pmatrix} \begin{pmatrix} \mathcal{F}^{(0)} \\ \mathcal{F}^{(1)} \end{pmatrix}, \quad (27)$$

where $\mathcal{F}^{(0)}$ and $\mathcal{F}^{(1)}$ are the anomalous amplitudes in the diagonal basis. The larger eigenvalue, say, $\lambda^{(0)}$, determines T_c and can be eliminated together with ϵ_c . The smaller eigenvalue $\lambda^{(1)}$ can be parametrized by the cutoff-independent quantity

$$\Lambda = \frac{\lambda^{(0)}\lambda^{(1)}}{\lambda^{(0)} - \lambda^{(1)}}. \quad (28)$$

We solve the set of equations (18,19,25,26) along with the gap equations for the order parameters selfconsistently.

After selfconsistency has been achieved, the LDOS in each band can be calculated by

$$\begin{aligned} N_\sigma(\epsilon, \vec{R})/N_{F\sigma} &= -\text{Im} \langle g_\sigma(\epsilon, \vec{p}_{F\sigma}, \vec{R}) \rangle_{\vec{p}_{F\sigma}}/\pi, \\ N_\pi(\epsilon, \vec{R})/N_{F\pi} &= -\text{Im} g_\pi(\epsilon, \vec{R})/\pi, \end{aligned} \quad (29)$$

where g_α is the upper diagonal (1,1) element of \hat{g}_α .

The current density around the vortex has contributions from both the σ and the π band. The corresponding expressions are

$$\begin{aligned} \frac{\vec{j}_\sigma(\vec{R})}{2eN_{F\sigma}} &= \int_{-\infty}^{\infty} \frac{d\epsilon}{2\pi} \langle \vec{v}_{F\sigma} \text{Im} g_\sigma \rangle_{\vec{p}_{F\sigma}} \tanh\left(\frac{\epsilon}{2T}\right), \\ \frac{\vec{j}_\pi(\vec{R})}{2eN_{F\pi}} &= \frac{\mathbb{D}}{\pi} \int_{-\infty}^{\infty} \frac{d\epsilon}{2\pi} \text{Im} [f_\pi^* \partial f_\pi] \tanh\left(\frac{\epsilon}{2T}\right). \end{aligned} \quad (30)$$

In our model, the bulk behaviour of the system is completely specified by four material parameters, ρ_0 , n_π/n_σ , T_c , and Λ . Here ρ_0 is the zero-temperature bulk gap ratio, $\rho_0 = \Delta_\pi^{\text{bulk}}/\Delta_\sigma^{\text{bulk}}$, and $n_\alpha = N_{F\alpha}/(N_{F\sigma} + N_{F\pi})$. For MgB₂, $\rho_0 \approx 0.3$ and $n_\pi/n_\sigma \approx 1 - 1.2$ [5, 10, 37]. The zero-temperature gap equations for a homogeneous system relate Λ with ρ_0 , n_π/n_σ , and the bulk gap ratio near T_c [2]. From this relation we find that for MgB₂, Λ can be positive or negative [38, 39, 40, 41] and can be close to zero [39]. Negative Λ implies that the effective Coulomb interaction dominates over the effective pairing interaction in the subdominant $\lambda^{(1)}$ channel, and in this case superconductivity is purely induced in the π band (with $\Delta_\pi > 0$, while $\Delta^{(1)} < 0$).

In the presence of inhomogeneity, there is another material parameter, namely ξ_π/ξ_σ , where $\xi_\sigma \simeq 6.8$ nm ($T_c = 39$ K) for MgB₂ [2]. As discussed in the next section, to reproduce the experimental data of ref. [5] we find $\xi_\pi/\xi_\sigma \approx 2$, for $\rho_0 = 0.3$ and $n_\pi/n_\sigma = 1$. The condition for the π band to be in the dirty limit so that the Usadel equation is applicable is $\xi_\pi/\xi_\sigma < 5$ for MgB₂ [2]. We present results for $\rho_0 = 0.1, 0.3, 0.5$; $\xi_\pi/\xi_\sigma = 1, 3, 5$; $n_\pi/n_\sigma = 1, 1.2$; and $\Lambda = -0.1, 0, 0.1$; and discuss the effects of induced superconductivity and hybridization of the diffusive and ballistic bands. For a given cell radius r_c , the corresponding field strength is given by equation (6) in units of $\hbar c/|e|\xi_\sigma^2$, which is about 13 T for MgB₂.

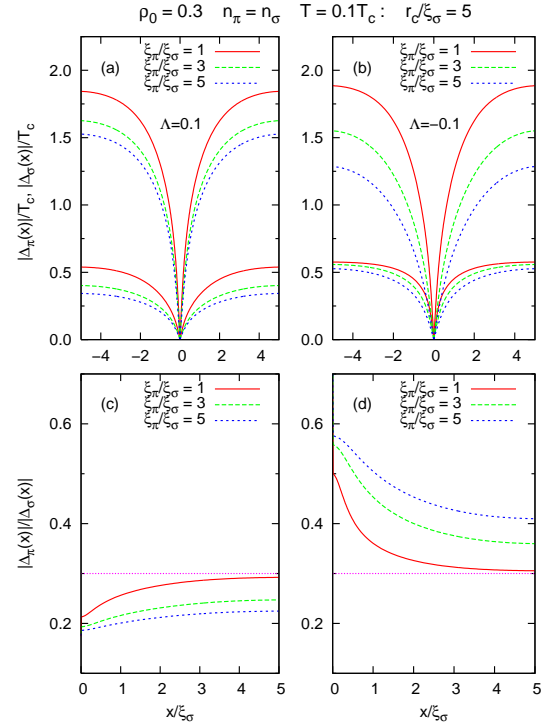


FIG. 1: Order parameters $|\Delta_\pi(x)|$ and $|\Delta_\sigma(x)|$ and their ratio as a function of coordinate x along a path through the vortex centre for $\xi_\pi/\xi_\sigma = 1, 3, 5$, $\rho_0 = 0.3$, $n_\pi = n_\sigma$, $T = 0.1T_c$, $r_c/\xi_\sigma = 5$, for $\Lambda = 0.1$ (a,c) and -0.1 (b,d).

III. RESULTS

A. Order parameter

In figure 1 we show the order parameter magnitudes in the two bands (a,b) and their ratio (c,d) as a function of coordinate x along a path through the vortex centre for $\rho_0 = 0.3$, $n_\pi = n_\sigma$, and $T = 0.1T_c$, for various values of the coherence length ratio ξ_π/ξ_σ ; for $\Lambda = 0.1$ (a,c) and -0.1 (b,d). The unit cell radius $r_c/\xi_\sigma = 5$ corresponds roughly to 0.5 T for MgB₂. The vortex structure is affected significantly by the Coulomb interaction and the impurity scattering rate in the π band. For $\Lambda > 0$, $|\Delta_\pi(x)/\Delta_\sigma(x)|$ is smaller than the bulk gap ratio ρ_0 in the vortex core. While for $\xi_\pi/\xi_\sigma = 1$ the ratio recovers more or less to the bulk value at the cell boundary, as ξ_π/ξ_σ increases, $|\Delta_\pi(x)|$ is suppressed more strongly and $|\Delta_\pi(x)/\Delta_\sigma(x)|$ is smaller than ρ_0 in the entire unit cell (for $\xi_\pi \sim r_c$). Furthermore, through coupling with the dirty π band, suppression of the σ -band order parameter by magnetic field is also enhanced for larger ξ_π/ξ_σ . This suppression of the order parameter and enlargement of the core area in the σ band with increasing ξ_π/ξ_σ are more drastic when the Coulomb repulsion is dominant in the π band ($\Lambda < 0$). Interestingly, in this case, the depletion of $|\Delta_\pi(x)|$ is relatively small and $|\Delta_\pi(x)/\Delta_\sigma(x)|$ is substantially larger than ρ_0 , especially for larger ξ_π/ξ_σ .

Changes in the order parameter magnitudes in the two

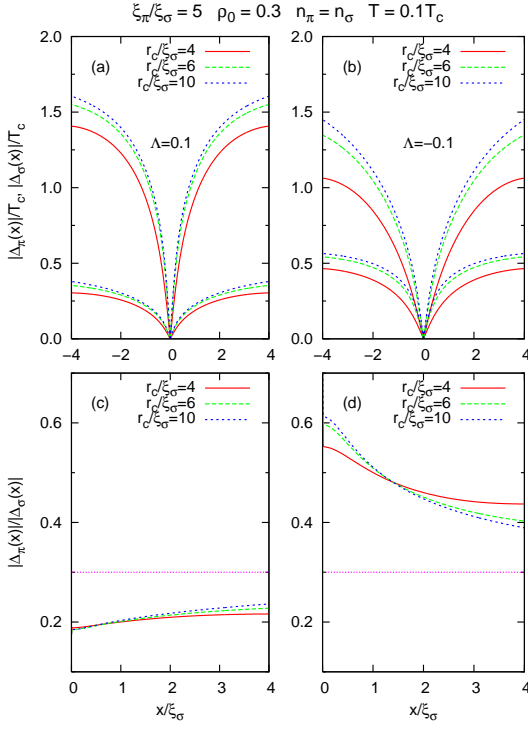


FIG. 2: Order parameters $|\Delta_\pi(x)|$ and $|\Delta_\sigma(x)|$ and their ratio as a function of coordinate x along a path through the vortex centre for $\xi_\pi/\xi_\sigma = 5$, $\rho_0 = 0.3$, $n_\pi = n_\sigma$, $T = 0.1T_c$, $r_c/\xi_\sigma = 4, 6, 10$, for $\Lambda = 0.1$ (a,c) and -0.1 (b,d).

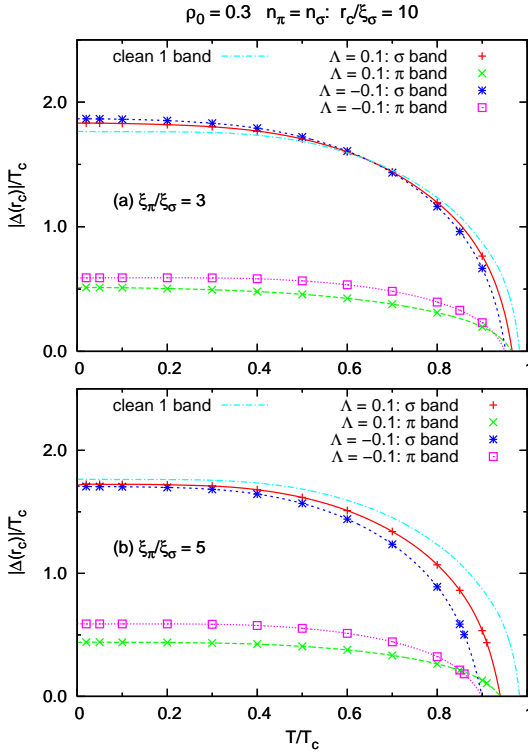


FIG. 3: Order parameter magnitude at the vortex unit cell boundary in the two bands as a function of temperature T for $\rho_0 = 0.3$, $n_\pi = n_\sigma$, $\Lambda = \pm 0.1$, $r_c/\xi_\sigma = 10$, for (a) $\xi_\pi/\xi_\sigma = 3$ and (b) 5. The result for a single clean band is also shown.

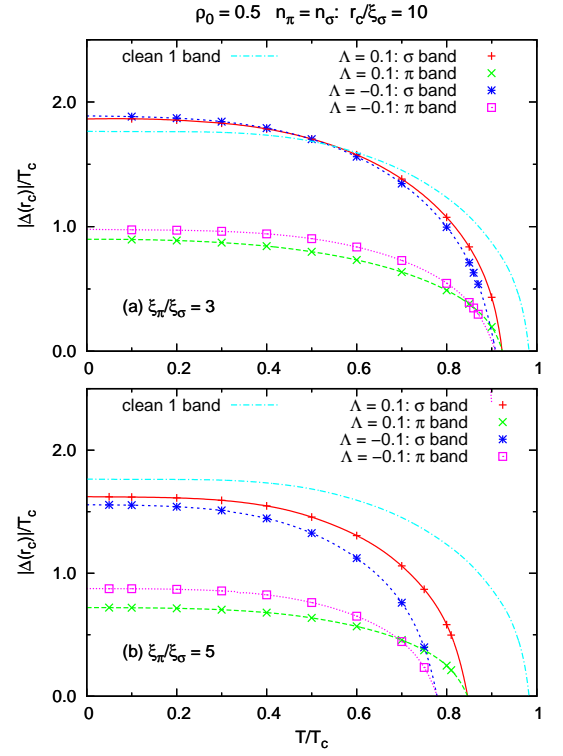


FIG. 4: Same as figure 3 except for $\rho_0 = 0.5$.

bands and their ratio as the field strength changes are illustrated in figure 2, for $\xi_\pi/\xi_\sigma = 5$, $\rho_0 = 0.3$, $n_\pi = n_\sigma$, and $T = 0.1T_c$, for various values of r_c ; for $\Lambda = 0.1$ (a,c) and -0.1 (b,d). The result for $r_c/\xi_\sigma = 10$ is similar to that for an isolated vortex. It can be seen clearly that for $\Lambda > 0$, the π -band order parameter is suppressed strongly by magnetic field and the core area is enlarged. In contrast, for $\Lambda < 0$, the depairing effect is more manifest in the σ band, with $|\Delta_\pi(x)|/|\Delta_\sigma(x)|$ reaching about two times ρ_0 in the vortex centre. It is clear that, while superconductivity is (mostly) induced in the π band, Coulomb interactions can renormalise substantially the length scales and the core sizes in the two bands in different ways.

We illustrate the influence of the diffusivity in the π band on the critical temperature in figures 3 ($\rho_0 = 0.3$) and 4 ($\rho_0 = 0.5$) for $n_\pi = n_\sigma$ and $r_c/\xi_\sigma = 10$, for (a) $\xi_\pi/\xi_\sigma = 3$ and (b) 5. In these figures the order parameter magnitudes at the cell boundary, $|\Delta(r_c)|$, in the two bands are plotted as a function of T for $\Lambda = 0.1$ and -0.1 , along with that for a single clean band. Points are results obtained by selfconsistent calculation and curves are guides to the eye. In a single ballistic band, the critical temperature where $|\Delta(r_c)|$ vanishes is slightly smaller than the zero-field T_c . When the ballistic σ band is coupled with the diffusive π band, the critical temperature is reduced further, and superconductivity is more suppressed by magnetic field for $\Lambda = -0.1$ than for $\Lambda = 0.1$. This difference is enhanced for larger ξ_π/ξ_σ , as a result of stronger suppression of the σ -band order parameter

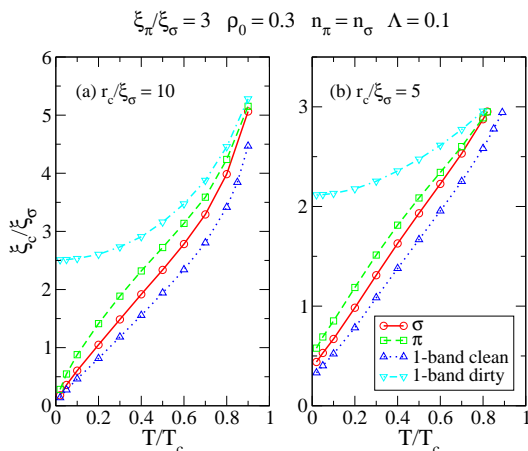


FIG. 5: Vortex core size as defined by equation (31) in the two bands as a function of temperature T for $\xi_\pi/\xi_\sigma = 3$, $\rho_0 = 0.3$, $n_\pi = n_\sigma$, $\Lambda = 0.1$, for (a) $r_c/\xi_\sigma = 10$ and (b) $r_c/\xi_\sigma = 5$. The results for a single clean and dirty band are also shown.

as discussed above. These effects of the diffusivity and the Coulomb interaction in the π band can be drastic when the coupling between the two bands is strong, as demonstrated for $\rho_0 = 0.5$ in figure 4.

A quantity to characterise the vortex core structure is the vortex core size defined by [42, 43]

$$\xi_c^{-1} = \frac{\partial \Delta(r=0)}{\partial r} \frac{1}{\Delta(r=\infty)}, \quad (31)$$

where r is the radial coordinate measured from the vortex centre, and $\Delta(r=\infty) \equiv \Delta(r_c)$ is the ‘bulk’ order parameter in the vortex lattice. Around an isolated vortex in a single clean band, the order parameter exhibits the KP effect [42], i.e., shrinkage of the vortex core size as T is lowered, approaching zero in the zero-temperature limit [43, 44, 45]. This is due to depopulation of higher-energy bound states in the vortex core. In an s -wave superconductor with nonmagnetic impurities, however, the core size as defined above saturates as T approaches zero [44, 45]. This stems from broadening of the bound core states that removes the singular behaviour in the spatial variation of the order parameter in the vortex core. The vortex core shrinking ceases when $k_B T$ becomes smaller than the energy width of the zero-energy bound states in the core.

When a ballistic band and a diffusive band are coupled, the KP effect is induced in the diffusive band, as found in refs. [2, 45] for an isolated vortex. In the vortex lattice, when vortices are well separated, one finds the KP effect in a single clean band as well as in coupled clean and dirty bands. This is demonstrated in figures 5 ($\Lambda = 0.1$) and 6 ($\Lambda = -0.1$), in which ξ_c in the two bands is plotted as a function of T for $\xi_\pi/\xi_\sigma = 3$, $\rho_0 = 0.3$, and $n_\pi = n_\sigma$, for (a) $r_c/\xi_\sigma = 10$ and (b) $r_c/\xi_\sigma = 5$. The core size in the case of a single clean and dirty band is also shown. As can be seen in figure 5(a), for $\Lambda > 0$, the core size in the π band is larger than that in the σ band for all temperature.

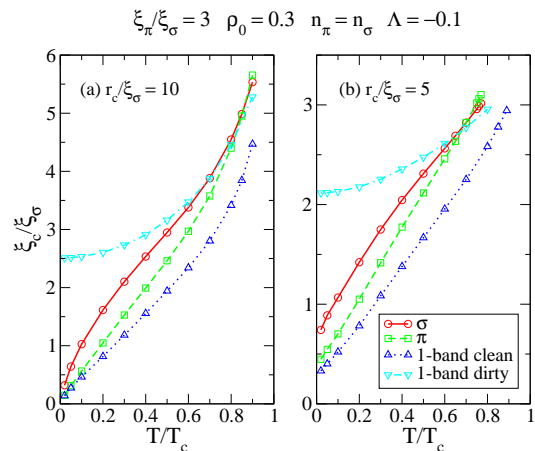


FIG. 6: Same as figure 5 except for $\Lambda = -0.1$.

$$\xi_\pi/\xi_\sigma = 3 \quad \rho_0 = 0.3 \quad n_\pi = n_\sigma \quad T/T_c = 0.1$$

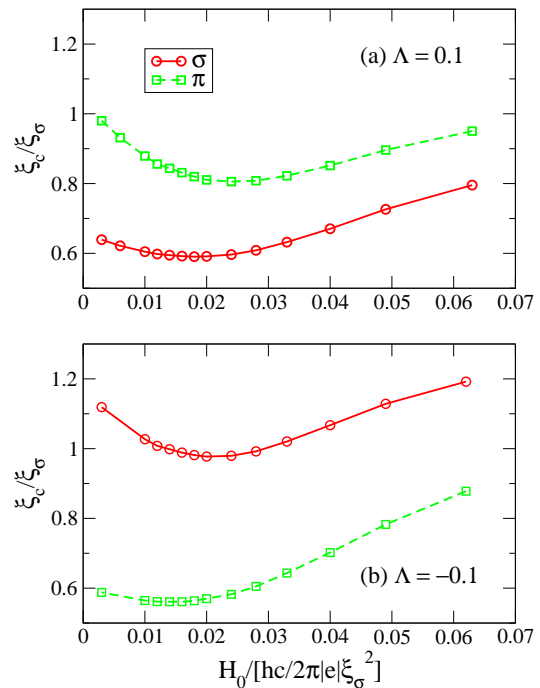


FIG. 7: Vortex core size as defined by equation (31) in the two bands as a function of field H_0 for $\xi_\pi/\xi_\sigma = 3$, $\rho_0 = 0.3$, $n_\pi = n_\sigma$, $T/T_c = 0.1$, for (a) $\Lambda = 0.1$ and $\Lambda = -0.1$.

The π -band order parameter exhibits the KP effect also when the Coulomb repulsion dominates (figure 6(a)), and in this case, ξ_c as defined above is always smaller in the π band than in the σ band (except for T very close to the critical temperature). Also note that, with dominating Coulomb interactions, the T -linear behaviour of the KP effect is better developed in the π band than in the σ band.

As magnetic field increases and vortices come closer together, the bound state wavefunctions of neighbouring vortices begin to overlap and form energy bands, and

quasiparticles can travel through the periodic array of vortices [11, 46, 47, 48] (see also references in ref. [11]). We have performed our calculation for the cell radius $r_c \geq 4$. For this range of r_c , we find that in a single diffusive band, the core size ξ_c becomes smaller as r_c decreases for any given temperature. Such shrinkage of the vortex core as field increases can be understood as due to intervortex transfer of quasiparticles [11], with higher-energy core bound states turning into extended states. This is also a trend for a single clean band as well as coupled ballistic and diffusive bands for relatively high T and relatively large r_c . However, as can be seen in figures 5(b) and 6(b), for relatively strong field, ξ_c is finite in the zero-temperature limit; since the derivative of the order parameter at the vortex centre remains finite as temperature approaches zero. Thus for a given (low) temperature, ξ_c can increase as a function of field strength above a certain critical value. This is illustrated in figure 7, where ξ_c is plotted as a function of field strength H_0 for $T/T_c = 0.1$, $\xi_\pi/\xi_\sigma = 3$, $\rho_0 = 0.3$, and $n_\pi = n_\sigma$, for (a) $\Lambda = 0.1$ and (b) $\Lambda = -0.1$. In both bands, as field increases, the core size is reduced initially, but at some critical strength it starts increasing. In a single ballistic band, ξ_c behaves similarly as a function of H_0 : this is consistent with the work by Miranović *et al* [49], who examined the effects of impurities on the vortex core size by including impurity scattering in the Eilenberger equation (single band). They have also found that for very small mean free path, the core size decreases monotonically as a function of field strength, as we find for a single diffusive band. In the case of two bands, ξ_c in the π band has nonmonotonic behaviour as in the σ band, and the low-temperature value of ξ_c is larger (smaller) in the π band than in the σ band for $\Lambda > 0$ (< 0).

B. Spectral properties of diffusive band

In the diffusive π band, the LDOS is completely flat as a function of energy at the vortex centre, as found for an isolated vortex [1, 2] and for coupled diffusive bands [25]. This is in agreement with the observation with STM [5]. The vortex core size as measured by a decay length of the zero-bias LDOS has also been probed by STM [5]. When superconductivity is (mostly) induced in a “weak” band in a coupled two-band system, such a decay length can be much larger in the “weak” band than in the “strong” band [1, 2, 24, 25]. We find that in the vortex state, there is little change in the zero-bias LDOS as a function of r in the σ band from that for an isolated vortex, except for rather small r_c . In contrast, as r_c is reduced, the π band starts exhibiting substantial overlap of quasiparticle states across the cell boundary for relatively large r_c . Furthermore, the LDOS decay length in the π band strongly depends on ρ_0 and ξ_π/ξ_σ . In figure 8 we present the zero-bias LDOS in the π band as a function of distance r from the vortex centre for $n_\pi = n_\sigma$, $T/T_c = 0.5$, $\Lambda = 0.1, 0, -0.1$, and $r_c/\xi_\sigma = 20$; for (a) $\rho_0 = 0.3$

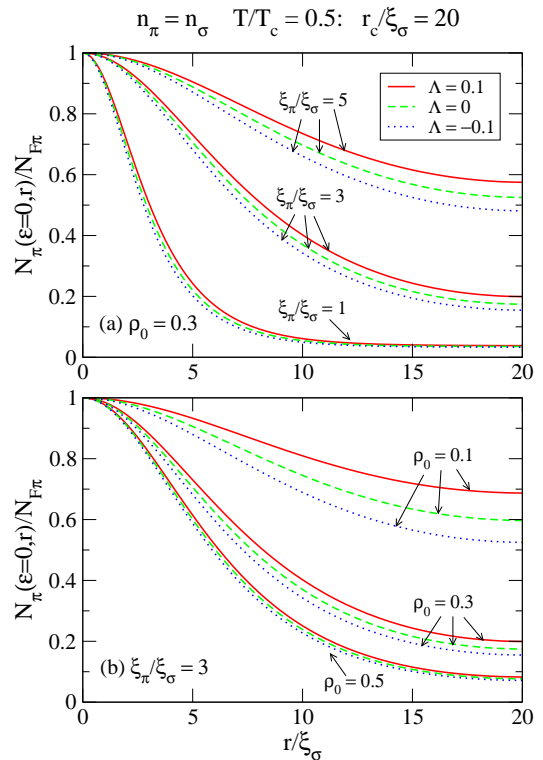


FIG. 8: Zero-bias LDOS in the π band as a function of distance r from the vortex centre for $n_\pi = n_\sigma$, $T/T_c = 0.5$, $\Lambda = 0.1, 0, -0.1$, $r_c/\xi_\sigma = 20$, for (a) $\rho_0 = 0.3$, $\xi_\pi/\xi_\sigma = 1, 3, 5$ and (b) $\xi_\pi/\xi_\sigma = 3$, $\rho_0 = 0.1, 0.3, 0.5$.

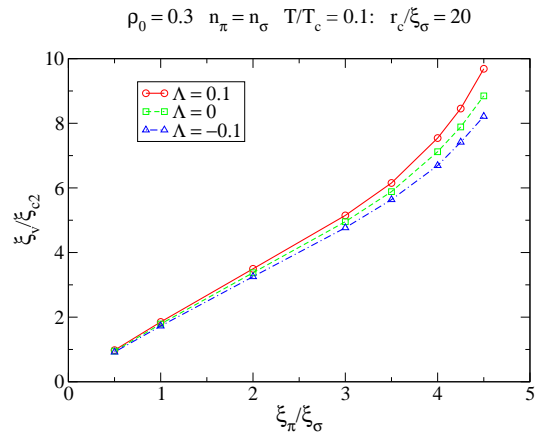


FIG. 9: Half-decay length ξ_v of the zero-bias LDOS in the π band as a function of ξ_π/ξ_σ for $\rho_0 = 0.3$, $n_\pi = n_\sigma$, $T/T_c = 0.1$, $r_c/\xi_\sigma = 20$, $\Lambda = 0.1, 0, -0.1$. For MgB₂, $\xi_{c2} = 10$ nm and the observed $\xi_v \approx 30$ nm corresponds to $\xi_\pi/\xi_\sigma \approx 2$ in our model.

various values of ξ_π/ξ_σ and (b) $\xi_\pi/\xi_\sigma = 3$ for several values of ρ_0 . For parameter values appropriate for MgB₂ ($\xi_\pi/\xi_\sigma \approx 2$, $\rho_0 = 0.3$; see below), the overlap of core states is not negligible already for $r_c/\xi_\sigma = 20$. For a fixed ρ_0 , the diffusivity in the π band (larger ξ_π/ξ_σ) enhances intervortex transfer of π -band quasiparticles. For

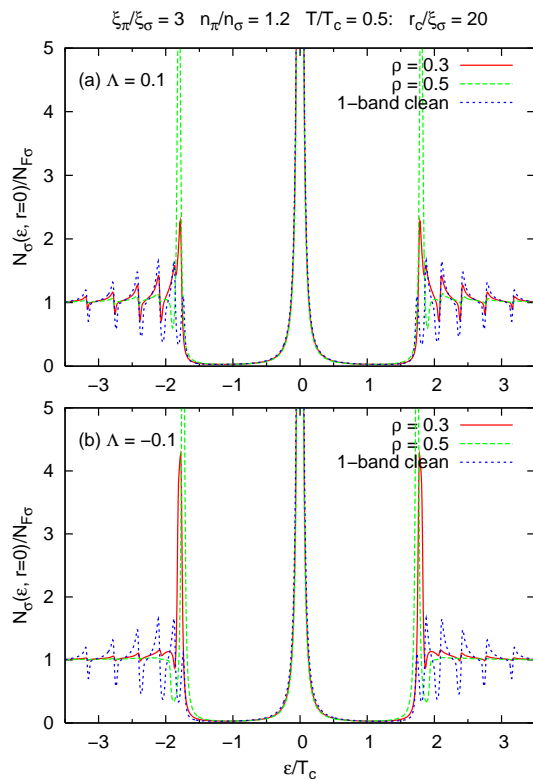


FIG. 10: Vortex centre spectra in the σ band as a function of energy ϵ for $\rho_0 = 0.3, 0.5$, $\xi_\pi/\xi_\sigma = 3$, $n_\pi/n_\sigma = 1.2$, $T/T_c = 0.5$, $r_c/\xi_\sigma = 20$, for (a) $\Lambda = 0.1$ and (b) -0.1 . The result for a single ballistic band is also shown.

a given ξ_π/ξ_σ , the weaker the induced superconductivity, the stronger the extension and overlap of quasiparticle states. The Coulomb repulsion in the π band (negative Λ) can enhance these effects further: e.g., for the parameter set for figure 8(b), the dependence of the LDOS on Λ is significant for $\rho_0 = 0.1$.

To characterise the core size, we plot in figure 9 the half-decay length of the zero-bias LDOS in the π band, ξ_v , in units of $\xi_{c2} \equiv 10$ nm (the Ginzburg-Landau coherence length in MgB₂ [5]) as a function of ξ_π/ξ_σ for $\rho_0 = 0.3$, $n_\pi = n_\sigma$, $T/T_c = 0.1$, and $r_c/\xi_\sigma = 20$. The ξ_v is a linear function of ξ_π/ξ_σ for $\xi_\pi/\xi_\sigma \lesssim 3$ in this example, and increases rapidly as ξ_π/ξ_σ increases further. Also for larger ξ_π/ξ_σ , its dependence on Λ becomes noticeable. For MgB₂, the experimental value of $\xi_v \approx 30$ nm corresponds to $\xi_\pi/\xi_\sigma \approx 2$ in our model. In ref. [25] such a plot of ξ_v was made for coupled dirty bands for $\xi_\pi/\xi_\sigma < 2.5$: overall ξ_v in this case is slightly smaller than our ξ_v .

C. Spectral properties of ballistic band

A particularly interesting feature found in our model of coupled ballistic and diffusive bands is that, through coupling with the “weak” diffusive band, there can be

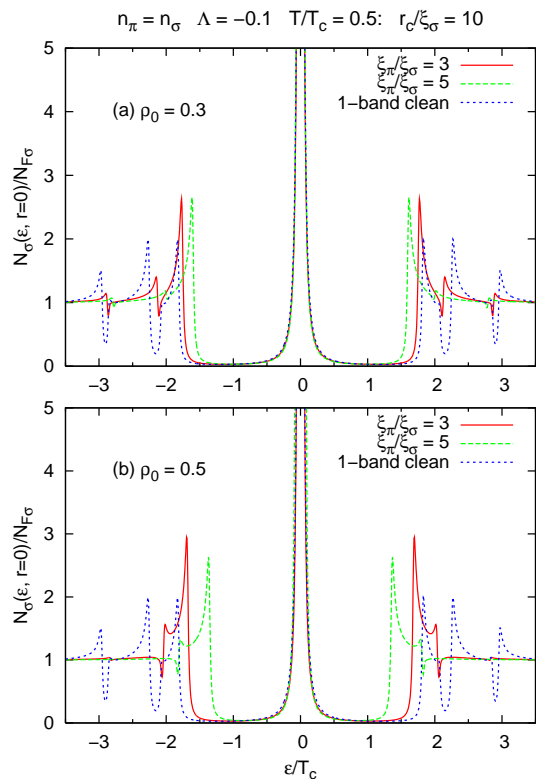


FIG. 11: Vortex centre spectra in the σ band as a function of energy ϵ for $\xi_\pi/\xi_\sigma = 3, 5$, $n_\pi = n_\sigma$, $\Lambda = -0.1$, $T/T_c = 0.5$, $r_c/\xi_\sigma = 10$, for (a) $\rho_0 = 0.3$ and (b) 0.5 . The result for a single ballistic band is also shown.

additional bound states at the gap edge in the “strong” ballistic band. We find such bound states for an isolated vortex [1, 2] as well as for the vortex lattice. In figure 10 the LDOS at the vortex centre in the σ band is plotted as a function of energy ϵ for $\rho_0 = 0.3, 0.5$, $\xi_\pi/\xi_\sigma = 3$, $n_\pi/n_\sigma = 1.2$, $T/T_c = 0.5$, and $r_c/\xi_\sigma = 20$; for (a) $\Lambda = 0.1$ and (b) -0.1 . We present in figure 11 the LDOS for $\xi_\pi/\xi_\sigma = 3, 5$, $n_\pi = n_\sigma$, $\Lambda = -0.1$, $T/T_c = 0.5$, and $r_c/\xi_\sigma = 10$; for (a) $\rho_0 = 0.3$ and (b) 0.5 . The result for a single ballistic band is also shown in these figures. The peak at $\epsilon = 0$ reflects the CdM bound states that arise from repeated Andreev scattering from the order parameter in the vortex core. In the core of an isolated vortex in a single clean band, the spectrum shows neither coherence peak nor additional bound state at the gap edge. In the vortex lattice, as quasiparticles travel in the periodic pairing potential, the continuum energy levels above the energy gap are grouped into bands and van Hove singularities appear at the band edges [48]. This can be seen clearly for a single ballistic band in figures 10 and 11: in the latter, the band widths are larger due to reduced lattice spacing.

When the ballistic σ band is coupled with the diffusive π band, the vortex core area is enlarged and the periodic pairing potential becomes effectively weaker. As a result, band gaps and van Hove singularities are reduced as can be seen in figures 10 and 11. At the same time,

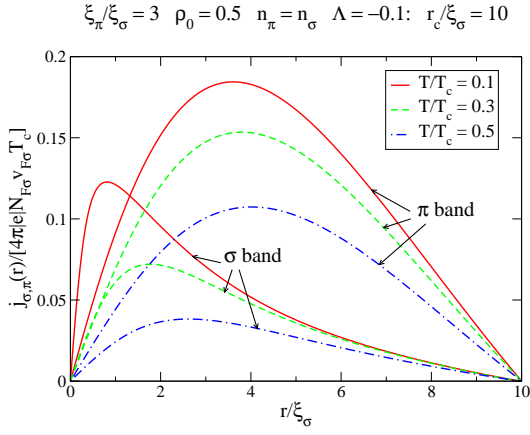


FIG. 12: Current density in the two bands as a function of distance r from the vortex centre for $\xi_{\pi}/\xi_{\sigma} = 3$, $\rho_0 = 0.5$, $n_{\pi} = n_{\sigma}$, $\Lambda = -0.1$, $r_c/\xi_{\sigma} = 10$, for $T/T_c = 0.1, 0.3, 0.5$.

extra bound states tend to appear at the gap edge. These features become prominent for larger ρ_0 (0.3 vs. 0.5 in figure 10) and ξ_{π}/ξ_{σ} (3 vs. 5 in figure 11), and are more enhanced for negative Λ than for positive Λ (figure 10). In most of the examples shown in these figures, the spectrum above the energy gap is more or less continuous. Furthermore, in the two-band results presented in figure 11(b), the energy gap is reduced substantially and a band of gap edge bound states is formed.

D. Current density

In figure 12 the current densities $j(r)$ in the two bands as a function of distance r from the vortex centre are shown for $\xi_{\pi}/\xi_{\sigma} = 3$, $\rho_0 = 0.5$, $n_{\pi} = n_{\sigma}$, $\Lambda = -0.1$, and $r_c/\xi_{\sigma} = 10$, for various temperatures. The current density contribution from the π band can be substantial, and even dominating as demonstrated in this figure, for larger ρ_0 and ξ_{π}/ξ_{σ} . As temperature is lowered, the σ -band current density exhibits the KP effect and is more confined around the vortex centre. For stronger coupling of the two bands, the KP effect becomes manifest also in the π band.

Deviation of the magnetic field distribution from the uniform field, $\delta H(r) = H(r) - H_0$, can be obtained from $j(r)$ by integrating the Maxwell equation, where a parameter $\kappa \equiv \sqrt{8\pi e^2 v_{F\sigma}^2 N_{F\sigma} / c^2} / \xi_{\sigma}$ comes in. For MgB_2 , $\kappa \approx 14$. The $\delta H(r)$ as a function of r is illustrated in figure 13 for $\xi_{\pi}/\xi_{\sigma} = 3$, $n_{\pi} = n_{\sigma}$, $\Lambda = -0.1$, $T/T_c = 0.1$, $r_c/\xi_{\sigma} = 10$, and $\kappa = 10$, for $\rho_0 = 0.3$ and 0.5. In figure 13(a) partial contribution from each band is shown, while 13(b) presents the total field distribution. It can be seen that when coupling of the two bands is increased, field fluctuations in the π band (hence those in the total field) are enhanced significantly, while the σ band contribution hardly changes.

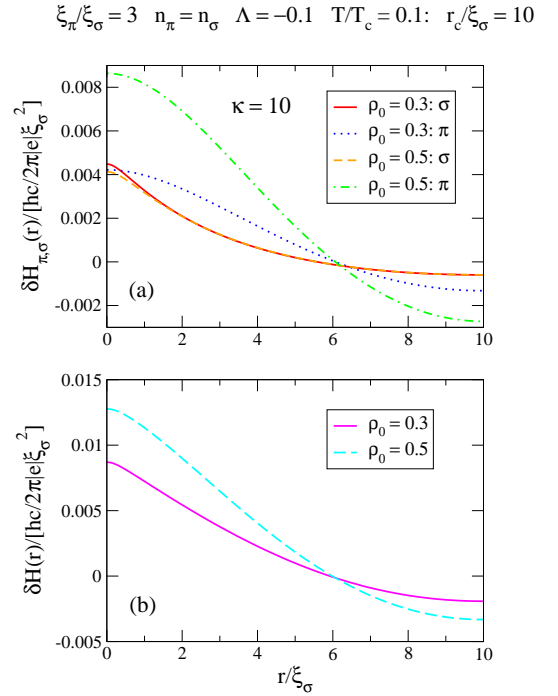


FIG. 13: Magnetic field distribution $\delta H = H - H_0$ as a function of distance r from the vortex centre for $\xi_{\pi}/\xi_{\sigma} = 3$, $n_{\pi} = n_{\sigma}$, $\Lambda = -0.1$, $T/T_c = 0.1$, $r_c/\xi_{\sigma} = 10$, for $\rho_0 = 0.3, 0.5$; (a) partial contribution from each band and (b) total field distribution. The $\kappa \equiv \sqrt{8\pi e^2 v_{F\sigma}^2 N_{F\sigma} / c^2} / \xi_{\sigma}$ that comes into the Maxwell equation is taken to be 10 ($\kappa \approx 14$ for MgB_2).

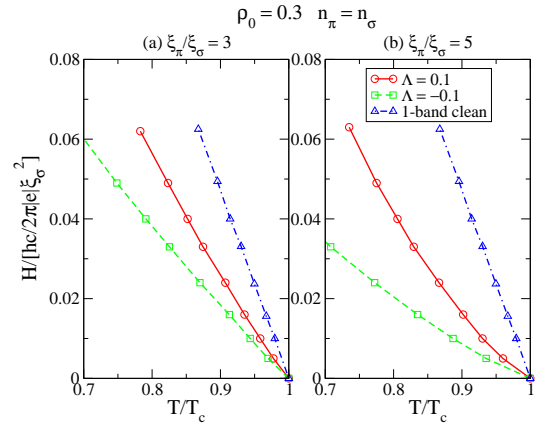


FIG. 14: Upper critical field as a function of temperature T for $\rho_0 = 0.3$, $n_{\pi} = n_{\sigma}$, $\Lambda = \pm 0.1$, for (a) $\xi_{\pi}/\xi_{\sigma} = 3$ and (b) 5. The result for a single clean band is also shown. The $\hbar c / |e| \xi_{\sigma}^2 \approx 13$ T for MgB_2 .

E. Phase diagram

We show in figure 14 the upper critical field $H_{c2}(T)$ for T near T_c for $\rho_0 = 0.3$, $n_{\pi} = n_{\sigma}$, and $\Lambda = \pm 0.1$, for (a) $\xi_{\pi}/\xi_{\sigma} = 3$ and (b) 5, along with the result for a single clean band. Although H_{c2} is sensitive to the amount of impurities in the sample, in MgB_2 single crys-

tals, H_{c2} for field parallel to the c axis has been measured to be $H_{c2}(T = T_c/2) \approx 2$ Tesla in several experiments [50, 51, 52, 53, 54, 55, 56, 57, 58, 59, 60]. This value roughly corresponds to Λ somewhere between -0.1 and 0.1 for $\xi_\pi/\xi_\sigma = 3$, $\rho_0 = 0.3$, and $n_\pi = n_\sigma$ in our model. When the σ band is coupled with the π band, H_{c2} is substantially reduced from the single-band value, and decreases further when the Coulomb repulsion dominates or the diffusivity increases in the π band. This is consistent with stronger suppression of the order parameter and enlargement of the vortex core area in the σ band. Furthermore, for relatively large ξ_π/ξ_σ , $H_{c2}(T)$ develops an upward curvature near T_c (figure 14(b)). This is interesting in light of the theoretical work based on the Eliashberg theory by Mansor and Carbotte, who studied the effects of Fermi velocity anisotropy and impurities on H_{c2} [61]. Their prediction for MgB₂ is that, for field in the c direction (where the Fermi velocities in the two bands are assumed to be the same), $H_{c2}(T)$ exhibits an upward curvature near T_c when the π band is clean and the σ band is dirty, while it has a quasilinear T dependence for the dirty π and the clean σ band (as observed in several experiments; see references in ref. [61]). Such an upward curvature in H_{c2} ($\parallel c$) has been observed in some experiments on MgB₂ single crystals [62, 63, 64].

IV. CONCLUSION

In conclusion, we have studied the effects of induced superconductivity and impurities on the electronic structure in the vortex lattice of a two-band superconductor, in which a “weak” 3D diffusive band and a “strong” 2D ballistic band are hybridized through the pairing interaction. We have found that the Coulomb repulsion and the diffusivity in the “weak” dirty band enhance suppression of the order parameter and enlargement of the vortex core by magnetic field in the “strong” clean band. As a result,

critical temperature and field (where the order parameter at the vortex unit cell boundary vanishes) are reduced, and increased diffusivity in the dirty band can result in an upward curvature of the upper critical field near the transition temperature. The Kramer-Pesch effect arising from thermal depopulation of higher-energy core bound states tends to disappear as field becomes stronger and overlap of quasiparticle states of neighbouring vortices increases. The zero-bias LDOS in the diffusive band has a decay length much larger than that in the ballistic band, indicating substantial intervortex transfer of quasiparticles, and the half-decay length increases significantly as the diffusivity increases. Coupling with the “weak” diffusive band leads to smearing of energy bands of the vortex lattice and van Hove singularities at the band edges in the vortex-core LDOS in the “strong” ballistic band. Furthermore, bound states tend to appear at the gap edge in the ballistic band, in addition to the well-known Carolide Gennes-Matricon bound states. These effects are enhanced for increased coupling, diffusivity, and Coulomb repulsion. Finally, the current density contribution in the vortex core and resulting field fluctuations in the diffusive band can be substantial, or even dominating, and exhibit the Kramer-Pesch effect manifest in the current density when coupling with the ballistic band is strong. We find the above intriguing features in the quasiparticle spectra for parameter values appropriate for MgB₂.

V. ACKNOWLEDGEMENTS

We thank A. E. Koshelev for helpful discussions and constructive comments on the manuscript. The research was supported by the Natural Sciences and Engineering Research Council of Canada, the Canada Foundation for Innovation, and the Deutsche Forschungsgemeinschaft within the CFN.

-
- [1] Tanaka K, Agterberg D F, Kopu J and Eschrig M 2006 *Phys. Rev. B* **73** 220501(R)
 - [2] Tanaka K, Eschrig M and Agterberg D F 2007 *Phys. Rev. B* **75** 214512
 - [3] Nagamatsu J, Nakagawa N, Muranaka T, Zenitani Y and Akimitsu J 2001 *Nature* **410** 63-64
 - [4] Schmidt H, Zasadzinski J F, Gray K E and Hinks D G 2002 *Phys. Rev. Lett.* **88** 127002
 - [5] Eskildsen M R, Kugler M, Tanaka S, Jun J, Kazakov S M, Karpinski J and Fischer Ø2002 *Phys. Rev. Lett.* **89** 187003; Eskildsen M R, Jenkins N, Levy G, Kugler M, Fischer Ø, Jun J, Kazakov S M and Karpinski J 2003 *Phys. Rev. B* **68** 100508(R)
 - [6] Geerk J, Schneider R, Linker G, Zaitsev A G, Heid R, Bohnen K-P and v Löhneysen H 2005 *Phys. Rev. Lett.* **94** 227005
 - [7] Giubileo F, Bobba F, Scarfato A, Cucolo A M, Kohen A, Roditchev D, Zhigadlo N and Karpinski J 2006 *Phys. Rev. B* **76** 024507
 - [8] Klein T, Lyard L, Marcus J, Holanova Z and Marcenat C 2006 *Phys. Rev. B* **73** 184513
 - [9] Serventi S, Allodi G, De Renzi R, Guidi G, Romanò L, Manfrinetti P, Palenzona A, Niedermayer Ch, Amato A and Baines Ch 2004 *Phys. Rev. Lett.* **93** 217003
 - [10] Sologubenko A V, Jun J, Kazakov S M, Karpinski J and Ott H R 2002 *Phys. Rev. B* **66** 014504
 - [11] Sonier J E 2004 *J. Phys.: Condens. Matter* **16** S4499-4513; Sonier J E 2007 *Rep. Prog. Phys.* **70** 1717-55
 - [12] Sonier J E, Hundley M F, Thompson J D and Brill J W 1999 *Phys. Rev. Lett.* **82** 4914-4917
 - [13] Miller R I, Kiefl R F, Brewer J H, Chakhalian J, Dunsiger S, Morris G D, Sonier J E and MacFarlane W A 2000 *Phys. Rev. Lett.* **85** 1540
 - [14] Boaknin E *et al* 2003 *Phys. Rev. Lett.* **90** 117003
 - [15] Callaghan F D, Laulajainen M, Kaiser C V and Sonier J E 2005 *Phys. Rev. Lett.* **95** 197001

- [16] Salman Z *et al* 2007 *Phys. Rev. Lett.* **98** 167001
- [17] Guritanu V, Goldacker W, Bouquet F, Wang Y, Lortz R, Goll G and Junod A 2004 *Phys. Rev. B* **70** 184526
- [18] Measson M-A, Braithwaite D, Flouquet J, Seyfarth G, Brison J P, Lhotel E, Paulsen C, Sugawara H and Sato H 2004 *Phys. Rev. B* **70** 064516
- [19] Seyfarth G, Brison J P, Méasson M-A, Flouquet J, Izawa K, Matsuda Y, Sugawara H and Sato H 2005 *Phys. Rev. Lett.* **95** 107004; Seyfarth G, Brison J P, Méasson M-A, Braithwaite D, Lapertot G and Flouquet J 2006 *Phys. Rev. Lett.* **97** 236403
- [20] Mukhopadhyay S, Sheet G, Raychaudhuri P and Takeya H 2005 *Phys. Rev. B* **72** 014545
- [21] Kasahara Y, Iwasawa T, Shishido H, Shibauchi T, Behnia K, Haga Y, Matsuda T D, Onuki Y, Sigrist M and Matsuda Y 2007 *Phys. Rev. Lett.* **99** 116402
- [22] Nakajima Y, Nakagawa T, Tamegai T and Harima H 2008 *Phys. Rev. Lett.* **100** 157001
- [23] Hunte F, Jaroszynski J, Gurevich A, Larbalestier D C, Jin R, Sefat A S, McGuire M A, Sales B C, Christen D K and Mandrus D 2008 *Nature* **453** 903
- [24] Nakai N, Ichioka M and Machida K 2002 *J. Phys. Soc. Jpn.* **71** 23-26; Ichioka M, Machida K, Nakai N and Miranović P 2004 *Phys. Rev. B* **70** 144508
- [25] Koshelev A E and Golubov A A 2003 *Phys. Rev. Lett.* **90** 177002
- [26] Caroli C, de Gennes P G and Matricon J 1964 *Phys. Lett.* **9** 307-9
- [27] Larkin A I and Ovchinnikov Y N 1968 *Zh. Eksp. Teor. Fiz.* **55** 2262-72 [1969 *Sov. Phys. JETP* **28** 1200-1205]
- [28] Eilenberger G 1968 *Z. Phys.* **214** 195-213
- [29] Usadel K 1970 *Phys. Rev. Lett.* **25** 507-509
- [30] Kramer L, Pesch W, and Watts-Tobin R J 1974 *J. Low. Temp. Phys.* **14** 29-51
- [31] Pesch W and Kramer L 1974 *J. Low. Temp. Phys.* **15** 367-386
- [32] Nagato Y, Nagai K, and Hara J 1993 *J. Low Temp. Phys.* **93** 33-56; Higashitani S and Nagai K 1995 *J. Phys. Soc. Jpn.* **64** 549-564; Nagato Y, Higashitani S, Yamada K and Nagai K 1996 *J. Low Temp. Phys.* **103** 1-22
- [33] Schopohl N and Maki K 1995 *Phys. Rev. B* **52** 490-493; Schopohl N 1998 Transformation of the Eilenberger Equations of Superconductivity to a Scalar Riccati Equation *Preprint* arXiv:cond-mat/9804064
- [34] Eschrig M, Sauls J A, and Rainer D 1999 *Phys. Rev. B* **60** 10447-10454
- [35] Eschrig M 2000 *Phys. Rev. B* **61** 9061-9076
- [36] Eschrig M, Kopu J, Konstandin A, Cuevas J C, Fogelström M and Schön G, 2004 *Adv. in Sol. State Phys.* **44** 533-546
- [37] Junod A, Wang Y, Bouquet F and Toulemonde P 2002 *Studies of High Temperature Superconductors*, edited by Narlikar A V vol 38 (Commack, NY: Nova Science) p 179
- [38] Szabó P, Samuely P, Kacmarčík J, Klein T, Marcus J, Fruchart D, Miraglia S, Marcenat C and Jansen A G M 2001 *Phys. Rev. Lett.* **87** 137005
- [39] Iavarone M *et al* 2002 *Phys. Rev. Lett.* **89** 187002
- [40] Gonnelli R S, Daghero D, Ummarino G A, Stepanov V A, Jun J, Kazakov S M and Karpinski J 2002 *Phys. Rev. Lett.* **89** 247004
- [41] Hol'ánová Z, Szabó P, Samuely P, Wilke R H T, Bud'ko S L and Canfield P C 2004 *Phys. Rev. B* **70** 064520
- [42] Kramer L and Pesch W 1974 *Z. Phys.* **269** 59-64
- [43] Kato Y and Hayashi N 2001 *J. Phys. Soc. Jpn.* **70** 3368-3376
- [44] Hayashi N, Kato Y and Sigrist M 2005 *J. Low. Temp. Phys.* **139** 79-96
- [45] Gumann A, Graser S, Dahm T and Schopohl N 2006 *Phys. Rev. B* **73** 104506
- [46] Canel E 1965 *Phys. Lett.* **16** 101-3
- [47] Klein U 1989 *Phys. Rev. B* **40** 6601-10
- [48] Pöttinger B and Klein U 1993 *Phys. Rev. Lett.* **70** 2806-2809
- [49] Miranović P, Ichioka M and Machida K 2004 *Phys. Rev. B* **70** 104510
- [50] Angst M, Puzniak R, Wisniewski A, Jun J, Kazakov S M, Karpinski J, Roos J and Keller H 2002 *Phys. Rev. Lett.* **88** 167004
- [51] Sologubenko A V, Jun J, Kazakov S M, Karpinski J and Ott H R 2002 *Phys. Rev. B* **65** 180505(R)
- [52] Zehetmayer M, Eisterer M, Jun J, Kazakov S M, Karpinski J, Wisniewski and Weber H W 2002 *Phys. Rev. B* **66** 052505
- [53] Lyard L *et al* 2002 *Phys. Rev. B* **66** 180502(R)
- [54] Angst M, Puzniak R, Wisniewski A, Roos J, Keller H, Miranović P, Jun J, Kazakov S M and Karpinski J 2003 *Physica C* **385** 143-153
- [55] Welp U *et al* 2003 *Physica C* **387** 137-142
- [56] Shi Z, Pradhan A K, Tokunaga M, Tamegai T, Takano Y, Togano K, Kito H and Ihara H 2003 *Physica C* **388-389** 157-8
- [57] Bando H, Yamaguchi Y, Shirakawa N and Yanagisawa T 2004 *Physica C* **412-414** 258-261
- [58] Eisterer M 2005 *Phys. Stat. Sol. C* **2** 1606-14
- [59] Kim H-J, Lee H-S, Byeongwon K, Yim W-H, Jo Y, Jung M-H and Lee S-I 2006 *Phys. Rev. B* **73** 064520
- [60] Klein T *et al* 2006 *Phys. Rev. B* **73** 224528
- [61] Mansor M and Carbotte J P 2005 *Phys. Rev. B* **72** 024538
- [62] Lee S, Mori H, Masui T, Eltsev Y, Yamamoto A and Tajima S 2001 *J. Phys. Soc. Jpn.* **70** 2255-2258
- [63] Xu M, Kitazawa H, Tanako Y, Ye J, Nishida K, Abe H, Matsushita A and Kido G 2001 *App. Phys. Lett.* **79** 2779-2781
- [64] Kim K H P *et al* 2002 *Phys. Rev. B* **65** 100510(R)